(μ-Phenoxo)$_2$Co^{II}M^{II} (M = Mn, Fe, Co) Core Complexes Having a "Co(salen)" Entity Embedded in a Macrocyclic Framework: Synthesis, Structure, and Properties

Hideki Furutachi and Hisashi Ōkawa*

Department of Chemistry, Faculty of Science, Kyushu University, Hakozaki, Higashiku, Fukuoka 812, Japan

Received January 17, 1997[⊗]

(μ-Phenoxo)$_2$Co^{II}M^{II} complexes, [CoM(L)(AcO)]ClO$_4$ (M = Mn (**1**), Fe (**2**), Co (**3**)) and [CoM(L)(NCS)]ClO$_4$ (M = Mn (**4**), Fe (**5**), Co (**6**)), have been obtained where $(L)^{2-}$ is a heterodinucleating macrocycle derived by the 2:1:1 condensation of 2,6-diformyl-4-methylphenol, ethylenediamine, and diethylenetriamine and has two dissimilar N_2O_2 and N_3O_2 metal-binding sites sharing the phenolic oxygens. The complex **1** crystallizes in the monoclinic space group $P2_1/n$, $a = 13.346(2)$ Å, $b = 10.093(2)$ Å, $c = 22.049(2)$ Å, $\beta = 104.58(1)°$, $V = 2874.3(7)$ Å^3, and $Z = 4$. The refinement converges with $R = 0.044$ and $R_w = 0.048$ for 2948 reflections with $|F_o| > 3\sigma(|F_o|)$. The Co(II) resides at the "salen"-like N_2O_2 site and the Mn(II) at the N_3O_2 site. The exogenous acetate group bridges the two metal ions in the $\eta^1{:}\eta^1$ mode together with the two phenolic oxygens, providing a square-pyramidal geometry about the Co(II) and a distorted six-coordinate geometry about the Mn(II). The Co--Mn intermetallic separation is 3.132(1) Å. The complexes **2** and **3** crystallize in the same triclinic space group $P\bar{1}$. **2**: $a = 10.632(3)$ Å, $b = 15.326(2)$ Å, $c = 9.499(2)$ Å, $\alpha = 106.64(1)°$, $\beta = 106.27(2)°$, $\gamma = 98.60(1)°$, $V = 1378.4(5)$ Å^3, and $Z = 2$. **3**: $a = 10.6047(9)$ Å, $b = 15.268(2)$ Å, $c = 9.571(1)$ Å, $\alpha = 107.262(10)°$, $\beta = 105.894(8)°$, $\gamma = 98.417(8)°$, $V = 1387.9(3)$ Å^3, and $Z = 2$. They have a dinuclear core similar to that of **1**. The complexes **4**, **5**, and **6** crystallize in the same monoclinic space group $P2_1/n$. **4**: $a = 14.486(2)$ Å, $b = 12.460(2)$ Å, $c = 15.728(1)$ Å, $\beta = 92.97(1)°$, $V = 2835.1(6)$ Å^3, and $Z = 4$. **5**: $a = 14.273(1)$ Å, $b = 12.438(2)$ Å, $c = 15.814(1)$ Å, $\beta = 93.279(7)°$, $V = 2802.8(6)$ Å^3, and $Z = 4$. **6**: $a = 14.257(3)$ Å, $b = 12.391(2)$ Å, $c = 15.801(2)$ Å, $\beta = 93.60(1)°$, $V = 2785.9(9)$ Å^3, and $Z = 4$. The refinement for **4** converges with $R = 0.065$ and $R_w = 0.064$ for 2174 reflections with $|F_o| > 3\sigma(|F_o|)$. The Co(II) resides at the N_2O_2 site and the Mn(II) at the N_3O_2 site. The Co--Mn separation bridged by the two phenolic oxygens is 3.175(2) Å. The thiocyanate group coordinates to the Mn(II) ion through its nitrogen atom and to the Co(II) ion of the neighboring complex through its sulfur atom, forming a 1-D infinite chain extended by the Mn−NCS−Co linkage. The geometry about the Co(II) is square-pyramidal with the thiocyanate sulfur at the apex, and that about the Mn(II) is of a distorted six-coordination. The complexes **5** and **6** are isomorphous with **4** in the Co--Fe and Co--Co separation of 3.172(1) and 3.101(2) Å, respectively. The magnetic studies reveal that the Co(II) at the N_2O_2 site is of high spin in the acetate complexes **1**−**3**, whereas it is of low spin in the thiocyanate complexes **4**−**6**. The M(II) ion at the N_3O_2 site assumes high-spin state in all of the complexes. The physicochemical properties of the complexes are examined and discussed on the basis of the molecular structures and the spin states of the Co(II) at the N_2O_2 site.

Introduction

Heterodinuclear metal complexes have been less studied compared with homodinuclear complexes, in spite of great interest in their properties arising from the presence of two dissimilar metal ions in close proximity. So far, considerable attention has been paid to magnetic interaction between two different metal ions, and such studies have served for understanding the spin-exchange mechanism in antiferro- or ferromagnetic interaction.[1,2] On the other hand, recent recognition of heterodinuclear cores at metallobiosites such as purple acid phosphatase (FeZn),[3] human calcineurin (FeZn),[4] and human protein phosphatase 1 (MnFe)[5] has stimulated interest in the cooperative functions of dissimilar metal ions of heterodinuclear metal systems.

In order to provide discrete heterodinuclear core complexes, it is recommended to use compartmental ligands whose two metal-binding sites are not equivalent with respect to cavity size, coordination number, or the nature of the donor atoms.[6] The phenol-based dinucleating macrocycle $(L)^{2-}$ (Chart 1), having two different metal-binding sites with the N_2O_2 and N_3O_2 donor sets sharing the two phenolic oxygens, has been developed in our laboratory.[7,8] It forms a series of Cu^{II}M^{II} and Ni^{II}M^{II} (M = Pb, Mn, Fe, Co, Ni, Cu, Zn) complexes having the Cu(II) or Ni(II) ion at the N_2O_2 site and the M(II) ion at the N_3O_2 site. One of our objects using $(L)^{2-}$ and related macrocycles is to provide heterodinuclear cores of functional significance. Of particular interest in this context is the dinuclear metal complexes with Mn(II), Fe(II), or Co(II) ion at the N_2O_2 site because this metal-binding site is compared to "salen" (*N*,*N*′-di-

[⊗] Abstract published in *Advance ACS Abstracts*, August 1, 1997.

(1) Kahn, O. *Struct. Bonding (Berlin)* **1987**, *68*, 89.
(2) Kahn, O. *Molecular Magnetism*; VCH: New York, 1993.
(3) Strater, N.; Klabunde, T.; Tucker, P.; Witzel, H.; Krebs, B. *Science* **1995**, *268*, 1489.
(4) Kissinger, C. R.; Parge, H. E.; Knighton, D. R.; Lewis, C. T.; Pelletier, L. A.; Tempczyk, A.; Kalish, V. J.; Tucker, K. D.; Showalter, R. E.; Moomaw, E. W.; Gastinel, L. N.; Habuka, N.; Chen, X.; Maldonado, F.; Barker, J. E.; Bacquet, R.; Villafranca, J. E. *Nature (London)* **1995**, *378*, 641.
(5) Egloff, M-P.; Cohen, P. T. W.; Reinemer, P.; Barford, D. *J. Mol. Biol.* **1995**, *254*, 942.
(6) Fenton, D. E.; Ōkawa, H. *Chem. Ber.*, in press.
(7) Ōkawa, H.; Nishio, J.; Ohba, M.; Tadokoro, M.; Matsumoto, N.; Koikawa, M.; Kida, S.; Fenton, D. E. *Inorg. Chem.* **1993**, *32*, 2949.
(8) Nishio, J.; Ōkawa, H.; Ohtsuka, S.; Tomono, M. *Inorg. Chim. Acta* **1994**, *218*, 27.

S0020-1669(97)00056-6 CCC: $14.00

Chart 1

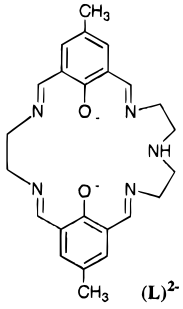

salicylideneethylenediaminate) and the salen complexes of these ions are reactive toward molecular oxygen.[9−11]

In this study, dinuclear $Co^{II}M^{II}$ (M = Mn, Fe, Co) complexes of $(L)^{2-}$, $[CoM(L)(AcO)]ClO_4$ (M = Mn (**1**), Fe (**2**), Co (**3**)) and $[CoM(L)(NCS)]ClO_4$ (M = Mn (**4**), Fe (**5**), Co (**6**)), have been prepared. The molecular structures, electronic structures, and physicochemical properties of the complexes are reported.

Experimental Section

Measurements. Elemental analyses of C, H, and N were obtained from the Service Center of Elemental Analysis at Kyushu University. Analyses of metals were made on a Shimadzu AA-680 atomic absorption−flame emission spectrophotometer. Infrared spectra were recorded on a JASCO IR-810 spectrophotometer using KBr disks. Electronic spectra were measured in *N*,*N*-dimethylformamide (DMF) (concentration: $\sim 1 \times 10^{-3}$ M) on a Shimadzu UV-210 spectrophotometer at room temperature. Magnetic susceptibilities were measured on a Faraday balance in the temperature range 80−300 K. Molar conductances were measured in DMF ($\sim 1 \times 10^{-3}$ M) on a DKK AOL-10 conductivity meter at room temperature. Fast atom bombardment (FAB) mass spectra were obtained on a JEOR JMS-SX102A/102A BE/BE four-sector type tandem mass spectrometer using nitrobenzyl alcohol as the matrix. Cyclic voltammograms were recorded on a BAS CV-50 electrochemical analyzer in DMF (1×10^{-3} M) containing tetraethylammonium perchlorate (TEAP, 1×10^{-1} M) as the supporting electrolyte (**CAUTION**: TEAP is explosive and should be handled with great care!). A three-electrode cell was used which was equipped with a glassy carbon working electrode, a platinum coil as the counter electrode, and a Ag/Ag^+ (TEAP/acetonitrile) reference electrode.

Preparations. The synthesis of the CoPb complex of the macrocycle $(L)^{2-}$, $[CoPb(L)(CH_3OH)(ClO_4)_2]$, was described in our preliminary report.[12] All of the operations for syntheses were carried out in an atmosphere of nitrogen using a glovebox from Vacuum Atmospheres Company, Model MO-40-IV, or in an atmosphere of argon using a standard Schlenk apparatus to avoid oxidation by atmospheric dioxygen.

$[CoM(L)(AcO)]ClO_4$ (1 (M = Mn), 2 (M = Fe), and 3 (M = Co)). These complexes were synthesized by a similar method. The synthesis of **1** is given. An acetonitrile solution (10 cm^3) of $[CoPb(L)(CH_3OH)(ClO_4)_2]$ (0.365 g, 0.4 mmol) and a methanol solution (2 cm^3) of $MnSO_4 \cdot 6H_2O$ (0.104 g, 0.4 mmol) were mixed and stirred for 10 min at room temperature. A methanolic solution (2 cm^3) of sodium acetate (0.03 g, 0.4 mmol) was added, and the mixture was refluxed for 1 h and evaporated to dryness. The residue was dissolved in acetonitrile (10 cm^3), insoluble $PbSO_4$ was separated by suction filtration, and the filtrate was evaporated to dryness. The resulting crude product was dissolved in DMF, and the solution was layered with 2-propanol to form red prisms.

Complex 1. Yield: 0.24 g (88%). μ_{eff} per CoMn: 7.58 μ_B at 290 K. FAB mass: *m*/*z* 590 for $\{CoMn(L)(AcO)\}^+$. Selected IR [ν/cm^{-1}] using KBr disks: 3340, 2930, 2860, 1660, 1640, 1560, 1410, 1145, 1100, 1080. Molar conductance [Λ_M/S cm^2 mol^{-1}] in DMF: 69. UV−vis [λ/nm (ϵ/M^{-1} cm^{-1})] in DMF: 362 (10 500), 460 (sh), 560 (990).

Complex 2: red prisms. Yield: 85%. μ_{eff} per CoFe: 5.70 μ_B at 290 K. FAB mass: *m*/*z*, 591 $\{CoFe(L)(AcO)\}^+$. Selected IR [ν/cm^{-1}] using KBr disks: 3330, 2910, 2850, 1650, 1630, 1550, 1405, 1140, 1100, 1080. Molar conductance [Λ_M/S cm^2 mol^{-1}] in DMF: 63. UV−vis [λ/nm (ϵ/M^{-1} cm^{-1})] in DMF: 358 (10 900), 460 (sh), 560 (1400).

Complex 3: red prisms. Yield: 82%. μ_{eff} per Co_2: 5.66 μ_B at 290 K. FAB mass: *m*/*z* 594 for $\{Co_2(L)(AcO)\}^+$. Selected IR [ν/cm^{-1}] using KBr disks: 3340, 2905, 2850, 1650, 1630, 1565, 1420, 1140, 110, 1080. Molar conductance [Λ_M/S cm^2 mol^{-1}] in DMF: 68. UV−vis [λ/nm (ϵ/M^{-1} cm^{-1})] in DMF: 365 (10 000), 480 (sh), 565 (1100).

$[CoM(L)(NCS)]ClO_4$ (4 (M = Mn), 5 (M = Fe) and 6 (M = Co)). The synthesis of **4** is described below. An acetonitrile solution (10 cm^3) of $CoPb(L)(CH_3OH)(ClO_4)_2$ (0.365 g, 0.4 mmol) and a methanol solution (2 cm^3) of $MnSO_4 \cdot 6H_2O$ (0.104 g, 0.4 mmol) were mixed and stirred for 10 min at room temperature. A methanol solution (2 cm^3) of sodium thiocyanate (0.03 g, 0.4 mmol) was then added, and the mixture was refluxed for 1 h and evaporated to dryness. The residue was dissolved in acetonitrile (20 cm^3), the solution was once filtered to separate $PbSO_4$, and the filtrate was evaporated to dryness. The resulting crude product was dissolved in DMF, and the solution was layered with 2-propanol to form red microcrystals.

Complex 4. Yield: 0.19 g (70%). μ_{eff} per CoMn: 5.93 μ_B at 290 K. FAB mass: *m*/*z* 589 for $\{CoMn(L)(NCS)\}^+$. Selected IR [ν/cm^{-1}] using KBr disks: 3325, 2910, 2850, 2070, 1658, 1635, 1140, 1105. Molar conductance [Λ_M/S cm^2 mol^{-1}] in DMF: 78. UV−vis [λ/nm (ϵ/M^{-1} cm^{-1})] in DMF: 370 (11 000), 540 (500).

Complex 5: red crystals. Yield: 73%. μ_{eff} per CoFe: 5.24 μ_B at 290 K. FAB mass: *m*/*z* 590 for $\{CoFe(L)(NCS)\}^+$. Selected IR [ν/cm^{-1}] using KBr disks: 3330, 2910, 2850, 2070, 1658, 1632, 1140, 1105, 1090. Molar conductance [Λ_M/S cm^2 mol^{-1}] in DMF: 74. UV−vis [λ/nm (ϵ/M^{-1} cm^{-1})] in DMF: 372 (10 900), 542 (800).

Complex 6: red crystals. Yield: 71%. μ_{eff} per Co_2: 4.72 μ_B at 290 K. FAB mass: *m*/*z* 593 for $\{Co_2(L)(NCS)\}^+$. Selected IR [ν/cm^{-1}] using KBr disks: 3340, 2910, 2850, 2070, 1650, 1630, 1140, 1105, 1080. Molar conductance [Λ_M/S cm^2 mol^{-1}] in DMF: 74. UV−vis [λ/nm (ϵ/M^{-1} cm^{-1})] in DMF: 362 (10 000), 542 (1100).

X-ray Crystallography. Each single crystal of **1**−**6** was mounted on a glass fiber and coated with epoxy resin. Measurements were made on a Rigaku AFC7R diffractometer with graphite-monochromated Mo Kα radiation (λ = 0.710 69 Å) and a 12 kW rotating anode generator. The data were collected at 20 ± 1 °C using an $\omega-2\theta$ scan technique to a maximum 2θ value of 50.0° at a scan speed of 16.0°/min (in ω). The weak reflections ($I < 10.0\sigma(I)$) were rescanned (maximum of four scans), and the counts were accumulated to ensure good counting statistics. Stationary background counts were recorded on each side of the reflection. The ratio of peak counting time to background counting time was 2:1. The diameter of the incident beam collimator was 1.0 mm, the crystal to detector distance was 235 mm, and the computer-controlled detector aperture was set to 9.0 × 13.0 mm (horizontal × vertical). The intensities of three representative reflections were measured after every 150 reflections. Over the course of the data collection, the standard reflections were monitored and the decay corrections were applied by a polynomial correction. An empirical absorption correction based on azimuthal scans of several reflections was applied. The data were corrected for Lorentz and polarization effects.

The structures were solved by a direct method and expanded using Fourier techniques. The non-hydrogen atoms were refined anisotropically. Hydrogen atoms were included in the structure factor calculation but not refined. Full-matrix least-squares refinements were based on observed reflections with $I > 3.00\sigma(I)$. Plots of $\sum w(|F_o| - |F_c|)^2$ vs $|F_o|$, reflection order in data collection, $\sin\theta/\lambda$, and various classes of indices showed no unusual trends. Crystal data and details of the structure determinations are summarized in Table 1.

Neutral atom scattering factors were taken from Cromer and Waber.[13] Anomalous dispersion effects were included in F_{calcd};[14] the values $\Delta f'$

(9) Larsen, E. J.; Pecoraro, V. L. *J. Am. Chem. Soc.* **1991**, *113*, 3810.
(10) Jones, R. D.; Summerville, D. A.; Basolo, F. *Chem. Rev.* **1979**, *79*, 137.
(11) Floriani, C.; Calderazzo, F. *Coord. Chem. Rev.* **1972**, *8*, 57.
(12) Shimoda, J.; Furutachi, H.; Yonemura, M.; Ohba, M.; Matsumoto, N.; Ōkawa, H. *Chem. Lett.* **1996**, 979.
(13) Cromer, D. T.; Waber, and J. T. *International Tables for X-ray Crystallography*; Kynoch Press: Birmingham, 1974; Vol. IV.
(14) Ibers, J. A.; Hamilton, W. C. *Acta Crystallogr.* **1964**, *17*, 781.

Table 1. Crystallographic Data for [CoM(L)(AcO)]ClO_4 (M = Mn (**1**), Fe (**2**), Co (**3**)) and [CoM(L)(NCS)]ClO_4 (M = Mn (**4**), Fe (**5**), Co (**6**))

	1	**2**	**3**	**4**	**5**	**6**
formula	$C_{26}H_{30}N_5O_8ClCoMn$	$C_{26}H_{30}N_5O_8ClCoFe$	$C_{26}H_{30}N_5O_8ClCo_2$	$C_{25}H_{27}N_6O_6ClSCoMn$	$C_{25}H_{27}N_6O_6ClSCoFe$	$C_{25}H_{27}N_6O_6ClSCo_2$
fw	689.88	690.78	693.87	688.91	689.82	692.90
cryst color	red	red	red	red	red	red
cryst size, mm	0.2 × 0.15 × 0.15	0.4 × 0.3 × 0.3	0.2 × 0.2 × 0.2	0.15 × 0.15 × 0.1	0.2 × 0.2 × 0.25	0.2 × 0.2 × 0.2
cryst syst	monoclinic	triclinic	triclinic	monoclinic	monoclinic	monoclinic
space group	$P2_1/n$	$P\bar{1}$	$P\bar{1}$	$P2_1/n$	$P2_1/n$	$P2_1/n$
a, Å	13.346(2)	10.632(3)	10.6047(9)	14.486(2)	14.273(1)	14.257(3)
b, Å	10.093(2)	15.326(2)	15.268(2)	12.460(2)	12.438(2)	12.391(2)
c, Å	22.049(2)	9.499(2)	9.571(1)	15.728(1)	15.814(1)	15.801(2)
α, deg	90	106.64(1)	107.262(10)	90	90	90
β, deg	104.58(1)	106.27(2)	105.894(8)	92.973(9)	93.279(7)	93.60(2)
γ, deg	90	98.60(1)	98.417(8)	90	90	90
V, Å^3	2874.3(7)	1378.4(5)	1387.9(3)	2835.1(6)	2802.8(6)	2785.9(9)
Z	4	2	2	4	4	4
D_{calcd}, g cm^{-3}	1.594	1.664	1.671	1.614	1.635	1.652
λ(Mo Kα), Å	0.71069	0.71069	0.71069	0.71069	0.71069	0.71069
no. of rflns	5608	4740	5153	5425	5400	5373
R,[a]	4.4	3.7	5.9	6.5	3.6	5.0
R_w,[b,c]	4.8	3.3	4.3	6.4	2.2	3.6

[a] $R = \sum||F_o| - |F_c||/\sum|F_o|$. [b] $R_w = \{\sum[w(|F_o| - |F_c|)^2]/\sum[w|F_o|^2]\}^{1/2}$. [c] $w = 1/\sigma^2(F_o)$.

and $\Delta f''$ were those of Creagh and McAuley.[15] The values for the mass attenuation coefficients are those of Creagh and Hubbel.[16] All of the calculations were performed on an IRIS Indigo computer using the teXsan crystallographic software package of Molecular Structure Corporation.[17] The final atomic coordinates of **1** and **4** are given in Tables 2 and 3, respectively. The atomic coordinates for the other complexes are available as Supporting Information.

Results and Discussion

Preparation. In our previous studies[7,8] the macrocyclic ligand $(L)^{2-}$ was obtained by the stepwise template reaction as the Cu^{II}Pb^{II} and Ni^{II}Pb^{II} complexes having the Cu(II) or Ni(II) ion at the N_2O_2 site and the Pb(II) ion at the N_3O_2 site. The CuPb and NiPb complexes were used as the precursors for a series of heterodinuclear Cu^{II}M^{II} and Ni^{II}M^{II} (M = Mn, Fe, Co, Ni, Cu, Zn) complexes, respectively. In a similar way, the CoPb complex CoPb(L)(CH_3OH)(ClO_4)$_2$ was obtained[12] which was used for the preparation of the Co^{II}M^{II} complexes in this study. The conversion of the CoPb complex into the CoM complexes was successfully achieved by transmetalation using metal(II) sulfate salts. In this reaction, the Pb(II) ion was eliminated as insoluble $PbSO_4$, and the CoM complexes were isolated as [CoM(L)(AcO)]ClO_4 (M = Mn (**1**); Fe (**2**); Co (**3**)) and [CoM(L)(NCS)]ClO_4 (M = Mn (**4**); Fe (**5**); Co (**6**)) in good yields.

It was shown on the basis of FAB mass spectrometry that the CoFe complexes **2** and **5** were contaminated with a small amount of the corresponding CoCo complex when prepared under refluxing conditions. The contamination of the impurity could be avoided when the transmetalation was carried out at ambient temperature. The CoMn complexes **1** and **4** were obtained without the contamination of the homonuclear impurity under refluxing conditions for transmetalation. In our attempts to prepare CoZn complexes, on the other hand, a scrambling of metal ions occurred to give a mixture of CoCo, CoZn, and ZnZn complexes even when reacted at ambient temperature.

Crystal Structures. [CoM(L)(AcO)]ClO_4 (1−3). The ORTEP[18] drawing of the cation of **1** (M = Mn) with 40% probability thermal ellipsoids is given in Figure 1 together with the atom-numbering scheme. The relevant bond distances and angles are given in Table 4.

The Co(II) ion resides at the salen-like N_2O_2 site, and the Mn(II) ion resides at the N_3O_2 site. The two metal ions are bridged by the phenolic oxygens O(1) and O(2) of the macrocycle $(L)^{2-}$ and the acetate group in the η^1:η^1 mode. The geometry about the Co is square-pyramidal with N(1), N(2), O(1), and O(2) of the macrocycle on the basal plane and O(4) of the acetate group at the apex. The basal donor atoms form a good coplane, and the Co is deviated 0.14 Å from the least-squares plane. The Co−N and Co−O bond distances (1.864(6)−1.916(4) Å) are compared to those of "Co(salen)" complexes.[19−22] The axial Co−O(4) bond distance (2.129(4) Å) is slightly elongated but significantly short relative to the axial Co−O bond in dimeric [Co(salen)]$_2$ (2.25−2.259 Å).[19,20]

The Mn at the N_3O_2 site assumes a distorted six-coordination. Because of the donation of the amino nitrogen N(4), the metal ion cannot reside within the basal cavity formed by O(1), O(2), N(3), and N(5). These donor atoms form a near coplane showing a slight distortion to a tetrahedron (the dihedral angle of O(1)−O(2) and N(3)−N(5) edges: 5.8°). The Mn is deviated 0.78 Å from the basal least-squares plane toward the acetate oxygen O(3). The acetate oxygen O(3) and the amino nitrogen N(4) are situated *cis* to each other. The Mn−L bond distances (2.221(5)−2.258(4) Å), except for the Co−O(3) (acetate) bond (2.099(4) Å), are significantly elongated relative to common high-spin Mn(II)−O and −N bonds.[23−25] The surroundings about the Mn can be depicted as a distorted trigonal prism where one triangular face is defined by N(3), N(4), and N(5) and the other face by O(1), O(2), and O(3). The two triangular faces are not parallel (the dihedral angle between the

(15) Creagh, D. C.; McAuley, W. J. In *International Tables for Crystallography*; Wilson, A. J. C., et al., Eds.; Kluwer Acad. Pub.: Boston, 1992; pp 219−222.
(16) Creagh, D. C.; Hubbell, J. H. In *International Tables for Crystallography*; Wilson, A. J. C., et al., Eds.; Kluwer Acad. Pub.: Boston, 1992; pp 200−206.
(17) TEXSAN, Molecular Structure Corporation, Houston, TX, 1985.
(18) Johnson, C. K. Report 3794, Oak Ridge National Laboratory, Oak Ridge, TN, 1965.
(19) Bruckner, S.; Calligaris, M.; Nardin, G.; Randaccio, L. *Acta Crystallogr. Sect. B* **1969**, *25*, 1671.
(20) Iasi, R. D.; Post, B.; Holt, S. L. *Inorg. Chem.* **1971**, *10*, 1498.
(21) Scjaeffer, W. P.; Marsh, R. E. *Acta Crystallogr. Sect. B* **1969**, *25*, 1675.
(22) Calligaris, M.; Minichelli, D.; Nardin, G.; Randaccio, L. *J. Chem. Soc. A* **1970**, 2411.
(23) Luneau, D.; Savariault, J.-M.; Cassoux, P.; Tuchagues, J.-P. *J. Chem. Soc., Dalton Trans.* **1995**, 275.
(24) Chang, H.-R.; Larsen, S. K.; Boyd, P. D. W.; Pierpont, C. G.; Hendrickson, D. N. *J. Am. Chem. Soc.* **1988**, *110*, 4565.
(25) Ikawa, Y.; Nagata, T.; Maruyama, K. *Chem. Lett.* **1993**, 1049.

Table 2. Final Atomic Coordinates of [CoMn(L)(AcO)]ClO_4 (**1**)

atom	*x*	*y*	*z*	B_{eq}[a]
Co(1)	−0.01664(6)	−0.18199(8)	−0.14544(4)	3.03(2)
Mn(1)	0.18131(7)	−0.35344(9)	−0.13925(4)	2.80(2)
Cl(1)	−0.3763(2)	−0.2849(2)	−0.1351(1)	5.99(6)
O(1)	0.0348(3)	−0.2847(4)	−0.2042(2)	3.19(9)
O(2)	0.0630(3)	−0.3020(4)	−0.0857(2)	3.04(9)
O(3)	0.2390(3)	−0.1592(4)	−0.1278(2)	3.6(1)
O(4)	0.1018(4)	−0.0353(4)	−0.1255(2)	4.5(1)
O(5)	−0.3408(7)	−0.2081(7)	−0.0806(3)	9.8(2)
O(6)	−0.3008(7)	−0.2814(9)	−0.1709(4)	12.9(3)
O(7)	−0.3912(5)	−0.4182(6)	−0.1183(3)	7.0(2)
O(8)	−0.4679(7)	−0.2394(8)	−0.1724(5)	13.0(3)
N(1)	−0.1055(4)	−0.0816(5)	−0.2072(3)	3.9(1)
N(2)	−0.0860(4)	−0.1031(5)	−0.0904(3)	3.4(1)
N(3)	0.2287(4)	−0.4860(5)	−0.0566(2)	3.3(1)
N(4)	0.3563(4)	−0.4171(6)	−0.1364(3)	3.9(1)
N(5)	0.1703(4)	−0.4858(5)	−0.2220(2)	3.3(1)
C(1)	−0.1536(6)	−0.3448(9)	−0.4646(3)	5.5(2)
C(2)	−0.1049(5)	−0.3280(7)	−0.3955(3)	3.7(2)
C(3)	−0.1361(5)	−0.2305(7)	−0.3607(3)	3.9(2)
C(4)	−0.0923(5)	−0.2135(6)	−0.2964(3)	3.4(1)
C(5)	−0.0106(4)	−0.2968(6)	−0.2647(3)	2.9(1)
C(6)	0.0223(5)	−0.3972(6)	−0.3005(3)	2.9(1)
C(7)	−0.0272(5)	−0.4112(7)	−0.3639(3)	3.5(2)
C(8)	−0.1323(5)	−0.1057(7)	−0.2655(3)	4.0(2)
C(9)	−0.1452(6)	0.0365(7)	−0.1806(4)	5.1(2)
C(10)	−0.1632(5)	−0.0026(7)	−0.1193(4)	4.6(2)
C(11)	−0.0751(5)	−0.1358(7)	−0.0328(3)	4.0(2)
C(12)	−0.0087(5)	−0.2381(6)	0.0004(3)	3.4(1)
C(13)	−0.0117(5)	−0.2635(7)	0.0631(3)	4.0(2)
C(14)	0.0445(5)	−0.3600(7)	0.0995(3)	3.9(2)
C(15)	0.0381(7)	−0.3850(8)	0.1658(4)	5.7(2)
C(16)	0.1093(5)	−0.4350(7)	0.0725(3)	3.6(2)
C(17)	0.1189(5)	−0.4149(6)	0.0113(3)	3.1(1)
C(18)	0.0572(4)	−0.3170(6)	−0.0269(3)	2.9(1)
C(19)	0.1969(5)	−0.4941(6)	−0.0069(3)	3.5(1)
C(20)	0.3210(6)	−0.5674(7)	−0.0566(3)	4.6(2)
C(21)	0.3989(5)	−0.4832(8)	−0.0767(3)	4.9(2)
C(22)	0.3560(6)	−0.5031(9)	−0.1911(3)	5.2(2)
C(23)	0.2573(6)	−0.5793(8)	−0.2130(3)	4.9(2)
C(24)	0.1068(5)	−0.4863(6)	−0.2766(3)	3.4(1)
C(25)	0.1955(5)	−0.0504(6)	−0.1192(3)	3.2(1)
C(26)	0.2643(6)	0.0676(7)	−0.1019(4)	5.0(2)

[a] $B_{eq} = (8/3)\pi^2(U_{11}(aa^*)^2 + U_{22}(bb^*)^2 + U_{33}(cc^*)^2 + 2U_{12}aa^*bb^* \cos\gamma + 2U_{13}aa^*cc^* \cos\beta + 2U_{23}bb^*cc^* \cos\alpha)$.

faces being 10.62°). Moreover, the N-based face is larger than the O-based face and both faces are deformed from a regular triangle.

The least-squares plane defined by O(1), O(2), N(1), and N(2) and the least-squares plane defined by O(1), O(2), N(3), and N(5) are bent at the O(1)−O(2) edge with a dihedral angle of 4.57°. Furthermore, the complex cation is bent at the Co−Mn edge, providing an umbrella shape for the "Co(salen)" entity and a saddle shape for the dinuclear core. The dihedral angle defined by the two aromatic rings is 31.31°. The bridging acetate group resides on the saddle. Such distortions of the structure surrounding the M(II), elongations in the M(II)−L bonds, and the bent core at the O(1)−O(2) and Co−M edges have been observed for the CuMn complex [CuMn(L)(AcO)]-BPh_4.[8]

The complexes **2** (M = Fe) and **3** (M = Co) differ from **1** in space group ($P\bar{1}$) but have an essentially similar core structure. Their relevant bond distances and angles are included in Table 4 for comparison. It must be mentioned that the Fe−L and Co−L bond distances in the N_3O_2 site are significantly long and compared to the Mn−L bond distances. Evidently the elongation of the M−L bonds arises from the geometric requirement of the N_3O_2 metal-binding site. The average of the M−O(1), M−O(2), M−N(3), and M−N(5) bond distances at the N_3O_2 site decreases slightly in the order **1** (Mn, 2.235 Å) > **2** (Fe, 2.169 Å) > **3** (Co, 2.148 Å) in accord with the ionic radii of the M(II) ions. Similarly, the M−N(4) and M−O(3) bond distances also decrease in this order. Interestingly, the average Co−L bond distances at the N_2O_2 site also decrease in this order, though the change is small.

Table 3. Final Atomic Coordinates of [CoMn(L)(NCS)]ClO_4 (**4**)

atom	*x*	*y*	*z*	B_{eq}[a]
Co(1)	−0.78042(8)	−0.01177(10)	−0.25749(7)	3.18(3)
Mn(1)	−0.95525(8)	−0.1300(1)	−0.34394(8)	2.95(3)
Cl(1)	−0.1604(2)	−0.5852(3)	−0.3457(2)	5.26(8)
S(1)	−0.7390(2)	−0.3317(2)	−0.1665(2)	4.93(7)
O(1)	−0.8110(4)	−0.0772(4)	−0.3646(3)	3.2(1)
O(2)	−0.9114(3)	0.0009(4)	−0.2508(3)	3.3(1)
O(3)	−0.1555(6)	−0.4863(7)	−0.3093(7)	12.3(4)
O(4)	−0.2514(5)	−0.6155(7)	−0.3682(5)	10.2(3)
O(5)	−0.1229(7)	−0.6572(9)	−0.2861(6)	13.9(4)
O(6)	−0.1060(6)	−0.5920(10)	−0.4141(5)	13.3(4)
N(1)	−0.6568(5)	−0.0513(6)	−0.2580(5)	3.6(2)
N(2)	−0.7524(5)	0.0367(6)	−0.1467(4)	3.7(2)
N(3)	−1.0896(4)	−0.0.577(5)	−0.3210(4)	3.2(2)
N(4)	−1.0679(5)	−0.2671(6)	−0.3842(4)	3.7(2)
N(5)	−0.9486(5)	−0.1441(6)	−0.4844(4)	3.8(2)
N(6)	−0.8924(5)	−0.2417(6)	−0.2540(4)	3.7(2)
C(1)	−0.5628(7)	−0.1379(10)	−0.6277(6)	6.7(3)
C(2)	−0.6263(7)	−0.1244(8)	−0.5571(6)	4.1(3)
C(3)	−0.5954(6)	−0.1063(8)	−0.4747(6)	4.3(3)
C(4)	−0.6536(6)	−0.0910(7)	−0.4073(5)	3.3(2)
C(5)	−0.7516(6)	−0.0963(7)	−0.4241(5)	3.2(2)
C(6)	−0.7831(6)	−0.1250(7)	−0.5074(5)	3.3(2)
C(7)	−0.7216(7)	−0.1368(8)	−0.5704(5)	4.3(3)
C(8)	−0.6131(6)	−0.0806(8)	−0.3222(7)	4.4(3)
C(9)	−0.6106(6)	−0.0508(9)	−0.1712(6)	5.1(3)
C(10)	−0.6522(6)	0.0361(8)	−0.1209(6)	4.7(3)
C(11)	−0.8092(7)	0.0744(8)	−0.0956(5)	4.5(3)
C(12)	−0.9097(6)	0.0839(7)	−0.1117(6)	3.7(2)
C(13)	−0.9593(7)	0.1264(8)	−0.0475(6)	4.7(3)
C(14)	−1.0538(8)	0.1378(8)	−0.0542(6)	5.3(3)
C(15)	−1.1077(7)	0.1860(8)	0.0152(7)	6.8(3)
C(16)	−1.0976(6)	0.0997(8)	−0.1281(6)	4.4(3)
C(17)	−1.0526(6)	0.0521(7)	−0.1920(5)	3.4(2)
C(18)	−0.9551(6)	0.0445(6)	−0.1880(5)	3.1(2)
C(19)	1.1113(5)	0.0042(7)	−0.2606(6)	3.6(2)
C(20)	−1.1690(6)	−0.1083(8)	−0.3687(6)	4.3(3)
C(21)	−1.1583(6)	−0.2286(7)	−0.3603(5)	4.0(3)
C(22)	−1.0672(6)	−0.2824(8)	−0.4774(7)	5.0(3)
C(23)	−1.0367(6)	−0.1476(7)	−0.5248(6)	4.9(3)
C(24)	−0.8791(7)	−0.1476(7)	−0.5314(5)	3.6(2)
C(25)	−0.8279(6)	−0.2776(7)	−0.2177(5)	3.1(2)

[a] $B_{eq} = (8/3)\pi^2(U_{11}(aa^*)^2 + U_{22}(bb^*)^2 + U_{33}(cc^*)^2 + 2U_{12}aa^*bb^* \cos\gamma + 2U_{13}aa^*cc^* \cos\beta + 2U_{23}bb^*cc^* \cos\alpha)$.

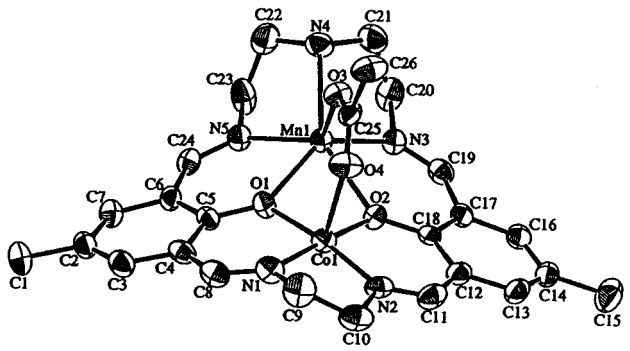

Figure 1. ORTEP drawing of the $\{CoMn(L)(AcO)\}^+$ part of **1** with the atom-numbering scheme.

Some geometrical features in the core of the acetate complexes **1**−**3** are summarized in Table 5. The tetrahedral distortion of the basal plane (ρ) of the N_3O_2 site becomes larger in the order **1** < **2** < **3**. Similarly the bending at the O(1)−O(2) edge (τ) becomes larger in this order. The Co--M intermetallic separation, the bending at the Co--M edge (ϕ), and

Table 4. Relevant Bond Distances (Å) and Angles (deg) of [CoM(L)(AcO)]ClO_4 (M = Mn (**1**), Fe (**2**), Co (**3**))

	1	2	3
	Distances		
Co(1)−O(1)	1.916(4)	1.897(2)	1.881(6)
Co(1)−O(2)	1.904(4)	1.904(2)	1.911(6)
Co(1)−O(4)	2.129(4)	2.131(3)	2.106(7)
Co(1)−N(1)	1.864(6)	1.872(3)	1.868(8)
Co(1)−N(2)	1.879(5)	1.871(3)	1.860(8)
M−O(1)	2.224(4)	2.176(2)	2.199(6)
M−O(2)	2.258(4)	2.204(2)	2.182(6)
M−O(3)	2.099(4)	2.036(2)	1.988(7)
M−N(3)	2.221(5)	2.142(3)	2.099(8)
M−N(4)	2.407(5)	2.361(3)	2.315(8)
M−N(5)	2.236(5)	2.155(3)	2.112(8)
	Angles		
O(1)−Co(1)−O(2)	83.7(2)	83.38(10)	82.7(3)
O(1)−Co(1)−O(4)	98.2(2)	97.78(10)	96.4(3)
O(1)−Co(1)−N(1)	94.0(2)	94.4(1)	94.5(3)
O(1)−Co(1)−N(2)	169.9(2)	166.5(1)	167.4(4)
O(2)−Co(1)−O(4)	92.5(2)	93.60(10)	93.7(3)
O(2)−Co(1)−N(1)	173.1(2)	173.1(1)	173.2(4)
O(2)−Co(1)−N(2)	95.9(2)	95.4(1)	95.8(3)
O(4)−Co(1)−N(1)	94.3(2)	93.1(1)	92.8(3)
O(4)−Co(1)−N(2)	91.9(2)	95.7(1)	96.2(3)
N(1)−Co(1)−N(2)	85.2(2)	85.2(1)	85.6(3)
O(1)−M−O(2)	69.4(1)	70.51(8)	69.8(2)
O(1)−M−O(3)	91.3(2)	95.48(9)	91.6(3)
O(1)−M−N(3)	137.6(2)	147.6(1)	150.2(3)
O(1)−M−N(4)	142.2(2)	134.2(1)	130.7(3)
O(1)−M−N(5)	78.1(2)	79.02(10)	79.6(3)
O(2)−M−O(3)	90.4(2)	88.80(9)	89.3(3)
O(2)−M−N(3)	78.5(2)	81.2(1)	83.5(3)
O(2)−M−N(4)	148.1(2)	152.1(1)	154.1(3)
O(2)−M−N(5)	130.8(2)	131.4(1)	129.6(3)
O(3)−M−N(3)	116.4(2)	99.5(1)	101.2(3)
O(3)−M−N(4)	85.5(2)	77.2(1)	75.9(3)
O(3)−M−N(5)	127.1(2)	132.0(1)	131.5(3)
N(3)−M−N(4)	75.2(2)	77.5(1)	78.8(3)
N(3)−M−N(5)	104.9(2)	110.3(1)	109.9(3)
N(4)−M−N(5)	74.1(2)	73.8(1)	74.7(3)
Co(1)−O(1)−M	98.1(2)	97.69(10)	98.6(3)
Co(1)−O(2)−M	97.3(2)	96.53(9)	98.3(3)

Table 5. Structural Parameters of [CoM(L)(AcO)]ClO_4 (M = Mn (**1**), Fe (**2**), Co (**3**))

	1	2	3
Co···M, Å	3.132(1)	3.0722(9)	3.101(2)
d(Co), Å[a]	0.14	0.17	0.16
d(M), Å[b]	0.78	0.63	0.62
ρ, deg[c]	5.8	13.0	15.9
τ, deg[d]	4.57	11.10	11.78
ϕ, deg[e]	31.31	26.29	27.47

[a] Deviation from the least-squares plane defined by O(1), O(2), N(1), and N(2). [b] Deviation from the least-squares plane defined by O(1), O(2), N(3), and N(5). [c] Tetrahedral distortion of the basal plane defined by O(1), O(2), N(3), and N(5). [d] The bending at the O(1)−O(2) edge between the plane defined by O(1), O(2), N(1), and N(2) and the plane defined by O(1), O(2), N(3), and N(5). [e] Dihedral angle between the two aromatic rings.

the deviation of Co from the basal least-squares plane show little change in **1**−**3**.

[CoM(L)(NCS)]ClO_4 (4−6). The ORTEP drawing of **4** (M = Mn) is given in Figure 2. The relevant bond distances and angles are given in Table 6.

X-ray crystallography has proved a similar dinuclear core with the Co(II) at the N_2O_2 site and the Mn(II) at the N_3O_2 site. The Co--Mn intermetallic separation doubly bridged by the phenolic oxygens O(1) and O(2) is 3.175(2) Å. A noticeable feature of this complex is the intermolecular bridge of the isothiocyanate group, forming a bond to the Mn(II) through its nitrogen and to the Co(II) of the adjacent molecule through its sulfur to

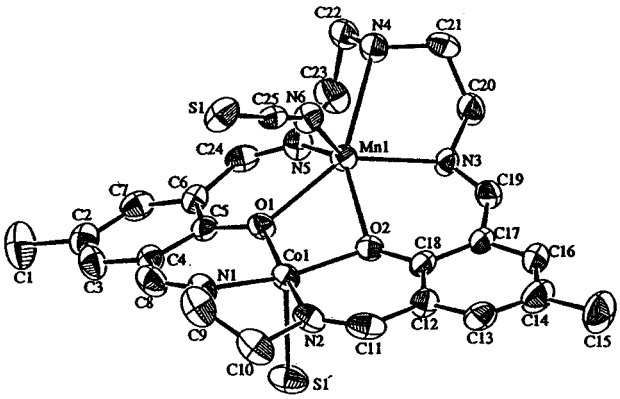

Figure 2. ORTEP drawing of the {CoMn (L)(NCS)}$^+$ part of **4** with the atom-numbering scheme.

Table 6. Relevant Bond Distances (Å) and Angles (deg) of [CoM(L)(NCS)]ClO_4 (M = Mn (**4**), Fe (**5**), Co (**6**))

	4	5	6
	Distances		
Co(1)−S(1′)[a]	2.565(3)	2.575(1)	2.585(3)
Co(1)−O(1)	1.902(5)	1.901(3)	1.895(6)
Co(1)−O(2)	1.913(5)	1.897(2)	1.891(6)
Co(1)−N(1)	1.856(7)	1.867(3)	1.863(7)
Co(1)−N(2)	1.869(7)	1.867(3)	1.863(7)
M−O(1)	2.231(5)	2.205(3)	2.214(6)
M−O(2)	2.259(5)	2.252(3)	2.250(6)
M−N(3)	2.194(7)	2.134(3)	2.082(7)
M−N(4)	2.423(7)	2.376(4)	2.355(8)
M−N(5)	2.222(7)	2.150(3)	2.112(7)
M−N(6)	2.151(7)	2.087(3)	2.068(8)
	Angles		
S(1′)−Co(1)−O(1)	89.3(2)	89.37(8)	89.9(2)
S(1′)−Co(1)−O(2)	95.0(2)	95.19(9)	95.5(2)
S(1′)−Co(1)−N(1)	95.7(2)	95.4(1)	94.9(2)
S(1′)−Co(1)−N(2)	97.3(2)	96.6(1)	96.9(2)
O(1)−Co(1)−O(2)	84.1(2)	83.4(1)	82.6(2)
O(1)−Co(1)−N(1)	93.7(3)	94.1(1)	95.2(3)
O(1)−Co(1)−N(2)	173.4(3)	174.0(1)	173.2(3)
O(2)−Co(1)−N(1)	169.0(3)	169.1(1)	169.3(3)
O(2)−Co(1)−N(2)	95.2(3)	95.9(1)	96.2(3)
N(1)−Co(1)−N(2)	85.8(3)	85.5(1)	84.7(3)
O(1)−M−O(2)	69.3(2)	69.07(9)	68.1(2)
O(1)−M−N(3)	138.5(2)	141.2(1)	142.6(3)
O(1)−M−N(4)	142.5(2)	140.9(1)	139.3(3)
O(1)−M−N(5)	77.8(2)	78.7(1)	79.5(3)
O(1)−M−N(6)	85.4(2)	84.3(1)	83.1(3)
O(2)−M−N(3)	79.6(2)	80.2(1)	81.7(3)
O(2)−M−N(4)	147.1(2)	147.8(1)	148.3(2)
O(2)−M−N(5)	132.5(3)	133.6(1)	133.6(3)
O(2)−M−N(6)	86.9(2)	85.4(1)	85.3(3)
N(3)−M−N(4)	75.0(2)	75.7(1)	76.9(3)
N(3)−M−N(5)	106.3(3)	108.8(1)	109.0(3)
N(3)−M−N(6)	120.5(3)	117.0(1)	116.8(3)
N(4)−M−N(5)	75.4(3)	75.3(1)	76.1(3)
N(4)−M−N(6)	88.4(3)	86.8(1)	83.9(3)
N(5)−M−N(6)	124.3(3)	124.4(1)	123.6(3)
Co(1)−O(1)−M	100.1(2)	100.9(1)	101.8(3)
Co(1)−O(2)−M	98.8(2)	99.4(1)	100.6(3)

[a] Symmetry code (′): $^1/_2 - x$, $^1/_2 + y$, $^1/_2 - z$.

provide an infinite chain extended by Mn−NCS−Co linkages (Figure 3). Thus, the Co at the N_2O_2 site assumes a square-pyramidal geometry with N(1), N(2), O(1), and O(2) of the macrocycle at the basal plane and S(1′) of the thiocyanate group at the apex. The equatorial bond distances are compared to those of the corresponding acetate complex **1**, whereas the apical Co−S(1′) bond is long (2.565(3) Å).

The Mn at the N_3O_2 site assumes a distorted six-coordinate geometry together with N(6) of the thiocyanate group. The structure about the metal is similar to that of **1** and can be

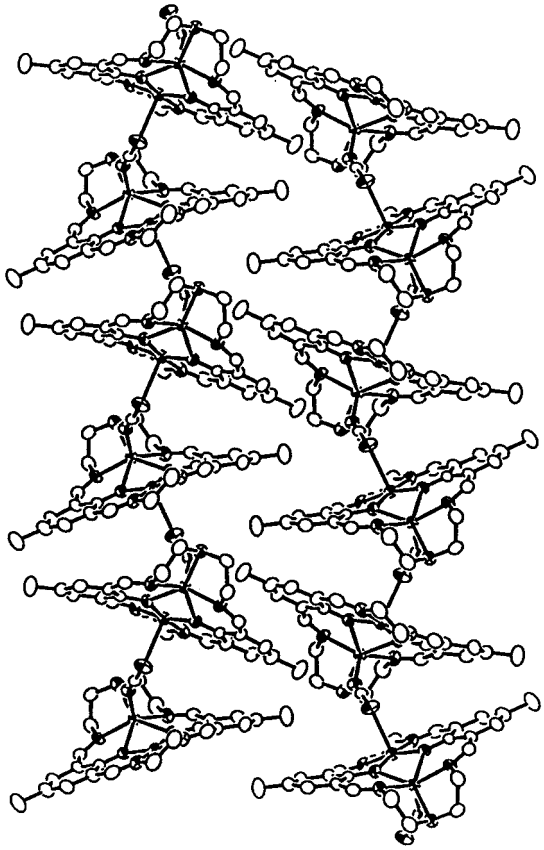

Figure 3. One-dimensional chain extended by the Mn−NCS−Co linkage running along the *b* axis.

Table 7. Structural Parameters of [CoM(L)(NCS)]ClO_4 (M = Mn (**4**), Fe (**5**), Co (**6**))

	4	**5**	**6**
Co···M, Å	3.175(2)	3.1717(8)	3.195(2)
d(Co), Å[a]	0.14	0.14	0.14
d(M), Å[b]	0.74	0.67	0.64
ρ, deg[c]	5.2	6.4	7.2
τ, deg[d]	9.57	10.88	11.13
ϕ, deg[e]	14.46	16.14	15.83

[a] Deviation from the least-squares plane defined by O(1), O(2), N(1), and N(2). [b] Deviation from the least-squares plane defined by O(1), O(2), N(3), and N(5). [c] Tetrahedral distortion of the basal plane defined by O(1), O(2), N(3), and N(5). [d] The bending at the O(1)−O(2) edge between the plane defined by O(1), O(2), N(1), and N(2) and the plane defined by O(1), O(2), N(3), and N(5). [e] Dihedral angle between the two aromatic rings.

depicted as a distorted trigonal prism. The basal plane defined by O(1), O(2), N(3), and N(5) is nearly coplanar with a small distortion to a tetrahedron (dihedral angle of 5.2°). The Mn−L bond distances are compared to those of the acetate complex **1**. Because of the intermolecular bridge of the thiocyanate group, the Co at the N_2O_2 site and the Mn at the N_3O_2 site are deviated by 0.14 and 0.74 Å, respectively, in the opposite direction.

The complexes **5** (M = Fe) and **6** (M = Co) are isomorphous with **4**. Their relevant bond distances and angles are included in Table 6. The average of the M−O(1), M−O(2), M−N(3), and M−N(5) bond distances decreases in the order **4** (Mn, 2.235 Å) > **5** (Fe, 2.169 Å) > **6** (M = Co, 2.148 Å). The M−N(4) bond distance decreases and the Co−S(1′) bond distance increases in this order.

Some geometrical features in the dinuclear core of the thiocyanate complexes **4**−**6** are summarized in Table 7. The distortion of the basal plane of the N_3O_2 site to a tetrahedron (ρ) and the bending at the O(1)−O(2) edge (τ) become larger in the order **4** < **5** < **6**. The deviation of the M(II) ion from the basal least-squares plane decreases in this order. The Co--M intermetallic separation, the bending of the core at the Co--M edge (ϕ), and the deviation of Co from the basal plane show little change in **4**−**6**.

Properties. IR Spectra. All of the complexes show two ν(C═N) vibrations in the region of 1650−1630 cm^{-1}, in harmony with the nonequivalent nature of the azomethine groups with respect to the two dissimilar metal-binding sites. The ν_{as}(COO) and ν_s(COO) modes of the acetate complexes **1**−**3** are seen at 1550−1565 and 1405−1420 cm^{-1}, respectively. The small separation between the two vibrations ($\Delta\nu$ < 150 cm^{-1}) is in accord with the bridging mode of the acetate group.[26] The thiocyanate complexes **4**−**6** show a ν(NC) vibration at ∼2070 cm^{-1}. The ν(SC) vibration is obscured by ligand IR bands and cannot be assigned definitely.

Magnetic Properties. The room-temperature magnetic moments of the complexes are given in the Experimental Section. It is found that the acetate complexes (**1**−**3**) have a large magnetic moment compared with the respective thiocyanate complexes (**4**−**6**). It is shown that the M(II) ion at the N_3O_2 site is always of high spin.[7,8] The spin-only magnetic moments of **1**−**6** (per CoM) are estimated on the basis of the expression $\mu^2 = \mu_{Co}^2 + \mu_M^2$, and using $\mu_{Co} = 3.88\ \mu_B$ for **1**−**3** and 1.73 μ_B for **4**−**6** as follows: 7.07 for **1**, 6.24 for **2**, 5.48 for **3**, 6.16 for **4**, 5.19 for **5**, and 4.24 for **6** μ_B. It is evident that each complex has a magnetic moment close to each spin-only value, demonstrating the high-spin state of the Co(II) ion in the acetate complexes and the low-spin state in the thiocyanate complexes.

A noticeable geometrical difference between the two classes is seen in the axial bond distance. In the acetate complexes **1**−**3**, the axial Co−O bond is the shortest (compressed square-pyramid), whereas in the thiocyanate complexes **4**−**6**, the axial Co−S bond is the longest (elongated square-pyramid). The effect of donor atom sets upon the spin state of a five-coordinate Co(II) complex has been well documented,[27] but this criterion cannot be applied to the complexes of "salen" and related quadridentate Schiff bases exhibiting a strong in-plane ligand field. Co(salen) and its analogs usually assume low spin, but axial coordination often provides a high spin ground state.[28,29]

Absorption Spectra. Electronic spectral data of **1**−**6** determined in DMF are given in the Experimental Section. It is important to know the complex structure in solution prior to spectroscopic discussion. The complexes **1**−**3** have a molar conductivity of 63−69 S cm^2 mol^{-1} in DMF, typical of 1:1 electrolytes in this solvent.[30] Evidently the acetate bridge is retained in DMF. Molar conductances of **4**−**6** are also typical of 1:1 electrolytes (74−78 S cm^2 mol^{-1}). It appears that the M−N(NCS) bond is retained but the Co−S bond is released in DMF. In the FAB mass spectra, the most prominent ion peak corresponds to $\{CoM(L)(X)\}^+$ (X = AcO or NCS) in all of the complexes (see Experimental Section).

The visible spectra of the acetate complexes **1**−**3** are similar and show an intense absorption band near 360 nm and moderately intense bands near 460 and 550 nm. The band near 360 nm with an extinction coefficient of ca. 1×10^4 M^{-1} cm^{-1} can be assigned to the $\pi-\pi^*$ transition associated with the

(26) Deacon, G. B.; Phillips, R. J. *Coord. Chem. Rev.* **1980**, *33*, 227.
(27) Sacconi, L. *Coord. Chem. Rev.* **1972**, *8*, 351.
(28) Migita, K.; Chikira, M.; Iwaizumi, M. *J. Chem. Soc., Dalton Trans.* **1983**, 2281.
(29) (a) Zarembowich, J.; Kahn, O. *Inorg. Chem.* **1984**, *23*, 589. (b) Zarembowich, J.; Claude, R.; Kahn, O. *Ibid.* **1985**, *24*, 1576. (c) Thuery, P.; Zarembowich, J. *Ibid.* **1986**, *25*, 2001.
(30) Geary, W. J. *Coord. Chem. Rev.* **1971**, *7*, 81.

azomethine linkage.[31] The absorption at ~550 nm has an extinction coefficient of ca. 1×10^3 M^{-1} cm^{-1}. The absorption at ~460 nm is barely observed as a discernible shoulder of the intense $\pi-\pi^*$ band; its intensity is estimated to be on the order of $\sim 1 \times 10^3$ M^{-1} cm^{-1} by subtracting the tail of the $\pi-\pi^*$ band. It must be emphasized that Co(salen) and its analogs show d−d transition bands of very weak intensity at longer wavelength.[32,33] Thus, the absorption bands at ~460 and ~550 nm cannot be assigned to d−d transition bands. A similar absorption is observed in the near ultraviolet region for alkoxo-[34,35] and phenoxo-bridged dinuclear copper(II) complexes,[36] and this is assigned to a charge-transfer (CT) transition from the filled p_π orbital of the bridging phenolic oxygen to the vacant d orbital of Cu(II). We tentatively assign the near ultraviolet bands observed for **1**−**3** to the CT transition bands from the filled p_π orbital of the phenolic oxygen to the vacant d orbitals of Co(II).

The absorption spectra of the thiocyanate complexes **4**−**6** show the azomethine $\pi-\pi^*$ transition band at ~370 nm and a moderately intense absorption band at ~540 nm. The latter band must have the same origin as the two bands found for **1**−**3**. The complexes **4**−**6** differ from **1**−**3** in the number of the CT band, and this fact may reflect the different spin state of the Co(II) ion.

Electrochemistry. Cyclic voltammograms of **1**−**6** are shown in Figure 4, and the numerical data are given in Table 8.

The acetate complexes **1** (M = Mn) and **3** (M = Co) are similar in cyclic voltammogram and show a reversible couple at ~−1.55 V (vs Ag/Ag$^+$) and a quasi-reversible couple at ~−0.35 V. They can be assigned to the Co(I)/Co(II) and Co(II)/Co(III) processes, respectively.[37,38] The M(II)/M(III) process does not occur in the available potential due to the distorted geometry about the M(II) and the long M(II)−L bond distances.[7,8] The acetate complex **2** (M = Fe) has another reversible wave at +0.05 V that is assigned to the Fe(II)/Fe(III) process.[7,8] This wave appears at low potential because of the electronically preferred d^5 configuration of Fe(III) ion.

The thiocyanate complexes **4** (M = Mn) and **5** (M = Co) resemble each other in cyclic voltammogram and show a reversible couple due to the Co(I)/Co(II) process at ~−1.25 V and an irreversible couple due to the Co(II)/Co(III) process at ~−0.23 V. The dissociation of the axial Co−S bond does not affect the Co(I)/Co(II) process because Co(I) in the low-spin d^8 electronic configuration prefers a planar geometry. On the other hand, the dissociation of the Co−S bond results in the irreversible Co(II)/Co(III) process because planar geometry is unfavorable for Co(III).

The complexes show another quasi-reversible couple near +0.35 V. It is unlikely that the replacement of the acetate oxygen (in **1** and **2**) with the thiocyanate nitrogen (in **4** and **5**) gives rise to a large shift (>0.7 V) in the redox potential of the M(II). Thus, this wave cannot be ascribed to the oxidation at the M(II) center. A promising candidate is thiocyanate ion that shows a redox couple in the region of +0.3 to +0.4 V. We presume that the thiocyanate group of **4** and **5** is more or less dissociated on electrode. The irreversible nature of the Co(II)/Co(III) process in **4** and **5** seems to be in harmony with the wave appearance at +0.35 V. In the case of **5** (M = Fe), the Co(II)/Co(III) wave shows good reversibility in accord with a small current at ~+0.35 V. This complex shows a reversible couple at +0.05 V due to the Fe(II)/Fe(III) redox process.

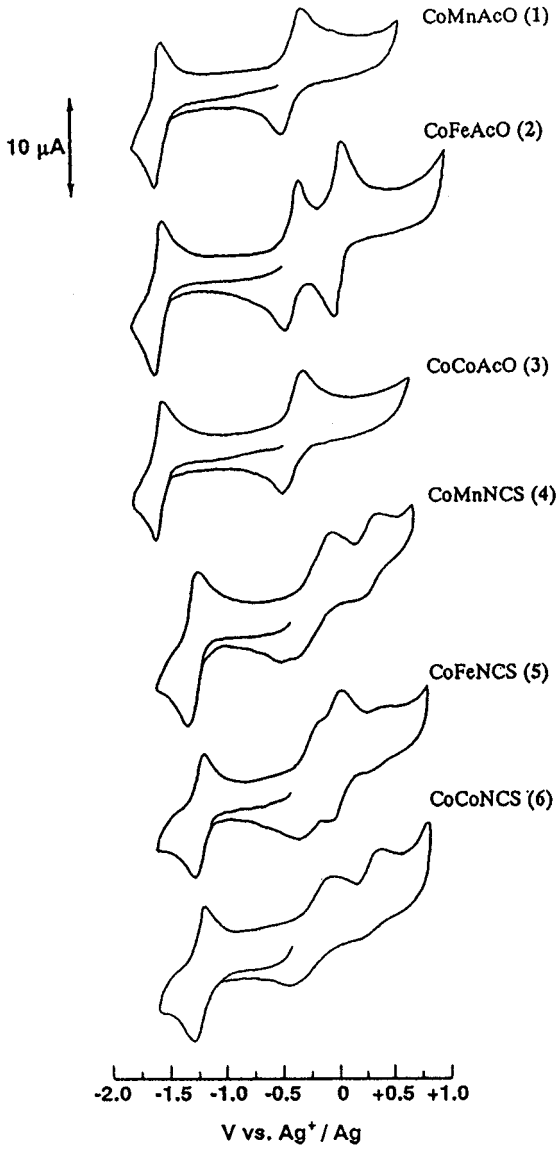

Figure 4. Cyclic voltammograms of **1**−**6**: glassy-carbon electrode, scan rate 50 mV s^{-1}, concentration 1×10^{-3} M, in DMF.

Table 8. Electrochemical Data of [CoM(L)(X)]ClO$_4$ Complexes (M = Mn, Fe, Co; X = AcO, NCS)[a]

	reduction $E_{1/2}$/V (ΔE/V)	oxidation $E_{1/2}$/V (ΔE/V)		
	Co(II)/Co(I)	Co(II)/Co(III)	M(II)/M(III)	
CoMnAcO (**1**)	−1.51 (0.07)	−0.34 (0.24)		
CoFeAcO (**2**)	−1.55 (0.06)	−0.35 (0.11)	+0.05 (0.07)	
CoCoAcO (**3**)	−1.57 (0.06)	−0.38 (0.19)		
CoMnNSC (**4**)	−1.27 (0.07)	−0.21 (0.34)		+0.36[b]
CoFeNCS (**5**)	−1.23 (0.06)	−0.22 (0.20)	+0.10 (0.09)	+0.43[b]
CoCoNCS (**6**)	−1.23 (0.06)	−0.26 (0.37)		+0.39[b]

[a] In DMF (concentration 1×10^{-3} M); supporting electrolyte TEAP (0.1 M); scan rate 50 mV/s; glassy-carbon working electrode; Pt auxiliary electrode; Ag/Ag$^+$ (TEAP/acetonitrile) reference electrode. [b] Anodic peak being given.

(31) Bosnich, B. *J. Am. Chem. Soc.* **1968**, *90*, 627.
(32) Busetto, C.; Cariati, F.; Fusi, A.; Gullotti, M.; Morazzoni, F.; Pasini, A.; Ugo, R.; Valenti, V. *J. Chem. Soc., Dalton Trans.* **1973**, 754.
(33) Hitchman, M. A. *Inorg. Chem.* **1977**, *16*, 1985.
(34) (a) Ishimura, Y.; Nonaka, Y.; Nishida, Y.; Kida, S. *Bull. Chem. Soc. Jpn.* **1973**, *46*, 3728. (b) Nishida, Y.; Kida, S. *Chem. Lett.* **1974**, 339.
(35) Mikuriya, M.; Nakamura, M.; Ōkawa, H.; Kida, S. *Chem. Lett.* **1982**, 839.
(36) Ōkawa, H.; Tadokoro, M.; Aratake, Y.; Ohba, M.; Shindo, K.; Mitsumi, M.; Koikawa, M.; Tomono, M.; Fenton, D. E. *J. Chem. Soc., Dalton Trans.* **1993**, 253.
(37) Costa, G.; Mestroni, G.; Puxeddu, A.; Reinhofer, E. *J. Chem. Soc. A* **1970**, *17*, 2870.
(38) Hammershmidt, R. F.; Broman, R. F. *J. Electroanal. Chem.* **1979**, *99*, 103.

It is noted that the potential for the acetate complexes **1**−**3** (−1.57 to −1.51 V) is about 0.3 V low relative to those of the thiocyanate complexes **4**−**6** (−1.27 to −1.23 V). This reflects the different spin states of the Co(II), indicating that high-spin Co(II) (for **1**−**3**) is hardly reduced compared to low-spin Co(II) (for **4**−**6**).

Acknowledgment. The authors thank Mr. Hitoshi Miyasaka of this laboratory for help with the magnetic measurements and X-ray crystallography and Dr. Hiroshi Sakiyama of Yamagata University for helpful discussion. This work was supported by a Grant-in-Aid for Scientific Research (No. 09440231) from the Ministry of Education, Science and Culture, Japan. Thanks are also due to The Daiwa Anglo-Japanese Foundation and The British Council for support.

Supporting Information Available: Analytical data for **1**−**6** (S1), tables listing detailed crystallographic data, atomic positional parameters, and bond lengths and angles of **1**−**6** (S2−S7), and ORTEP drawings of **2**, **3**, **5**, and **6** (S8−S11) (101 pages). Ordering information is given on any current masthead page.

IC9700563